Experimental Characterizations and Estimation of the Natural Frequency of Nonlinear Rubber-Damped Torsional Vibration Absorbers

Wen-Bin Shangguan
School of Mechanical and Automotive Engineering,
South China University of Technology,
Guangzhou 510641, China

Yiming Guo
School of Mechanical and Automotive Engineering,
South China University of Technology,
Guangzhou 510641, China

Yuming Wei
School of Mechanical and Automotive Engineering,
South China University of Technology,
Guangzhou 510641, China

Subhash Rakheja[1]
School of Mechanical and Automotive Engineering,
South China University of Technology,
Guangzhou 510641, China;
CONCAVE Research Center,
Mechanical & Industrial Engineering,
Concordia University,
Montreal, QC H4B 1R6, Canada
e-mail: 349733684@qq.com

Weidong Zhu
University of Maryland,
Baltimore County,
Baltimore, MD 21250

The natural frequency of a rubber-damped torsional vibration absorber (TVA) depends on the excitation amplitudes and frequencies in a highly nonlinear manner. This is due to nonlinear shear properties of the rubber ring. In this study, the nonlinear static and dynamic shear characteristics of a rubber ring, and the natural frequency of a nonlinear TVA are experimentally characterized firstly. Since a rubber ring employed in a rubber-damped TVA is usually in the compression state, its static and dynamic shear properties depend upon the compression ratio and dimensions apart from the chemical ingredients in a highly complex manner. The prediction of the natural frequency of a rubber-ring TVA thus poses considerable complexities. In this study, a special fixture is designed and fabricated for characterizing shear properties of a rubber ring subject to different compression ratios. The shear properties are subsequently characterized using different constitutive models, and a methodology for identifying the model parameters is presented considering the measured properties. Second, a methodology for estimating the natural frequency of the TVA is proposed, and the effectiveness of the proposed method is demonstrated through comparisons of the estimated natural frequency with the measured values. The results of the study suggest that the model using fractional derivatives to characterize nonlinear shear properties of a rubber ring can be effectively used to obtain accurate estimation of natural frequency of a nonlinear TVA over a wide range of excitations. The natural frequency of a TVA can thus be accurately estimated before prototyping using the experimental and modeling methods developed in this paper.
[DOI: 10.1115/1.4033579]

Keywords: torsional vibration absorbers, rubber damped, characterization of nonlinear natural frequency, modeling of rubbers properties, constitutive models

1 Introduction

Rotating machines such as compressors, turbines, and crankshaft in an internal combustion engines, invariably, exhibit torsional vibrations [1]. Various design constraints often cause the rotating shafts to undergo resonant oscillations at several critical speeds within the working speed range. The high magnitudes of torsional vibration corresponding to these critical speeds may lead to shaft failures, if not controlled. TVA such as centrifugal pendulum absorber, Houdaille damper, dry-friction damper, Frahm's absorber, and rubber dampers [2,3] are commonly used to dampen torsional vibration in the rotating machines. Among these, the rubber material damper is most widely used due to its relatively low cost, simple construction, and greater reliability [1,4]. This, in part, is due to developments for processing of rubber materials, which could be easily moulded to the desired shape and design specifications [5].

The developments in passive TVA and their applications have been widely reported during the past many decades. These may be grouped in four categories on the basis of the major focus or objectives: (i) studies reporting methods for realizing target natural frequency, damping, and moment of inertia (MOI) of a TVA to achieve optimal control of vibration of the primary system [1–4]; (ii) studies exploring applications of smart materials such as electrorheological or magnetorheological fluids in controllable TVAs [6,7]; (iii) studies investigating nonlinear transient dynamic responses of TVAs such as pendulum TVA [8,9]; and (iv) those exploring alternate concepts and TVA structures, such as pendulum or roller type absorbers [10].

The natural frequency of a rubber material damper is an important design parameter and its determination continues to be challenging due to nonlinear shear properties of the rubber rings. The dynamic properties of rubber materials used in TVAs have been described using widely different linear and nonlinear visco-elastic models. The models such as Kelvin–Voigt, Maxwell, and fractional derivate models have been commonly used for characterization of visco-elastic properties of rubber materials [11–15]. The excitation amplitude dependence of stiffness and damping properties of the rubber have been realized by introducing a friction element in the Maxwell and fractional derivate models, which have been widely used for characterization of nonlinear behaviors of rubber isolators of compression type (e.g., [16–20]). Berg [16] proposed a five-parameter model for characterizing mechanical behavior of a rubber spring in railway suspensions considering superposition of elastic, fractional, and viscous forces. Sjoberg and Kari [17,18] presented a nonlinear dynamic model integrating the shape factor-based stiffness, a fractional derivative, and a generalized friction model for describing properties of a cylindrical carbon-filled rubber isolator. An extension of the above-stated five-parameter fractional derivative model was further proposed for characterizing dynamic properties of a hydraulic engine mount [19,20].

A rubber-damped TVA generally consists of an inertia ring that absorbs the vibration energy, a rubber ring that provides essential

[1]Corresponding author.

Contributed by the Technical Committee on Vibration and Sound of ASME for publication in the Journal of Vibration and Acoustics. Manuscript received April 25, 2015; final manuscript received March 19, 2016; published online June 2, 2016. Assoc. Editor: Lei Zuo.

stiffness and damping properties, and a hub that couples the TVA to the rotating shaft [1,4,21]. During assembly, the rubber ring is usually forced into the gap between the inertia ring and the hub in an interference fit manner. The rubber ring pressed into the gap between the inertia ring and the hub of the TVA serves two functions: (i) provide torsional stiffness and damping and (ii) withstand torque applied to TVA when TVA is required to transmit power as in the case of torsional vibration damper used in the engine crankshaft. The rubber ring within the TVA thus remains in a compression state, whose properties cannot be accurately described by majority of the models described in the aforementioned studies. Since the shear properties of the rubber ring in a TVA are dependent upon its compression ratio and dimensions in a highly nonlinear manner, apart from the chemical properties [22], the prediction of natural frequency of a rubber TVA is quite complex. The reported analytical and numerical models of the rubber TVA generally consider dynamic shear modulus ranging from 1.5 to 3 MPa and Poisson's ratio near 0.49 [1], while the contributions due to variations in compression ratio (interference fit value), the chemical ingredients, and sizes of the rubber ring are mostly ignored.

The estimation of the natural frequency of a rubber-damped TVA involves experimental characterizations of highly nonlinear static and dynamic shear properties of rubber ring under wide ranges of compression and excitations. While the shear stress–strain properties of rubbers have been reported in a number of studies under different experimental conditions [23,24], to the best of our knowledge, the characterizations of static and dynamic properties of rubber rings under ranges of compression ratio have not been reported. A reliable method for predicting the natural frequency of a nonlinear rubber-damped TVA prior to prototyping thus does not yet exist. In the industry, the natural frequencies of the rubber TVAs are generally determined via repeated fabrications and measurements using different compression ratios, sizes, and shapes of the rubber ring. It has been shown that the natural frequency of a rubber-damped TVA is determined largely by the properties of the rubber ring and the external excitations. Developments of an experimental method for characterizing nonlinear shear properties and development of a systematic methodology for estimating natural frequency of a TVA over desired ranges of loading and excitation conditions are thus significant for realizing the designs of rubber-damped TVAs in an efficient manner.

This study presents experimental and modeling methods for characterizing nonlinear static and dynamic shear properties of a rubber ring subject to different compression ratios. The design of a test rig is presented for experimental characterizations of shear properties under different compression ratio and excitation conditions. The natural frequency of the nonlinear TVA under different excitations is also measured using the test system developed by Saginomiya Inc., Yokohama, Japan. A systematic methodology is further presented for estimating natural frequency of a nonlinear TVA over a range of loading and excitation conditions using laboratory-measured shear characteristics together with known visco-elastic models. The relative effectiveness of the models in estimating the natural frequency over a wide range of excitation amplitudes is demonstrated through comparisons of the estimated and measured natural frequencies. The relations between the natural frequency of the TVA and characteristics of rubber ring are illustrated. It is shown that the natural frequency can be accurately estimated using the proposed method prior to the prototype design, which can help engineer to choose sizes of rubber ring, compression ratio, and chemical compounds for mixing rubbers.

2 Characterization of Shear Properties of Rubber Specimens

Figure 1(*a*) illustrates a rubber-damped TVA employed for control of torsional vibration of engine crankshafts. The TVA comprises a hub, a rubber ring, and an inertia ring. The natural frequency of the TVA is determined from MOI of the inertia ring, and stiffness and damping properties of the rubber ring. The stiffness and damping of the rubber ring, however, are very difficult to obtain due to their nonlinear dependence on dimensions of the rubber ring, rubber compound, and compression ratio [25,26]. Experimental characterizations of shear properties of the rubber ring under a given compression ratio thus need to be characterized first for estimating natural frequency of the TVA.

2.1 Measurement of Shear Properties of Rubber Specimens.

A test fixture is designed for experimental characterization of static and dynamic shear characteristics of rubber specimens as shown in Fig. 1(*b*). The fixture includes a movable block (1), two clamping plates (2,10), two locking blocks (4,7), an intermediate block (5), two rubber specimens (8), a gaskets (9), and two sets of fastening bolts (3,6). The movable block (1) and the intermediate (5) and locking blocks (4,7) are connected to the moving and fixed ends of an elastomer test equipment (MTS 831), respectively. Two rubber specimens (8) are placed symmetrically between the two locking blocks (4,7) and the movable block (1), while the two locking blocks can be compressed by the two clamping plates (2,10). The compression ratio of the rubber specimens, defined as ratio of the compressed thickness to undeformed thickness, could be varied by using different thickness of the gaskets between the two clamping plates. Table 1 summarizes the undeformed specimen dimensions in terms of thickness d_0 and area A_0, together with the shore hardness.

An experiment was designed to characterize static and dynamic shear properties of the rubber specimen in terms of reaction

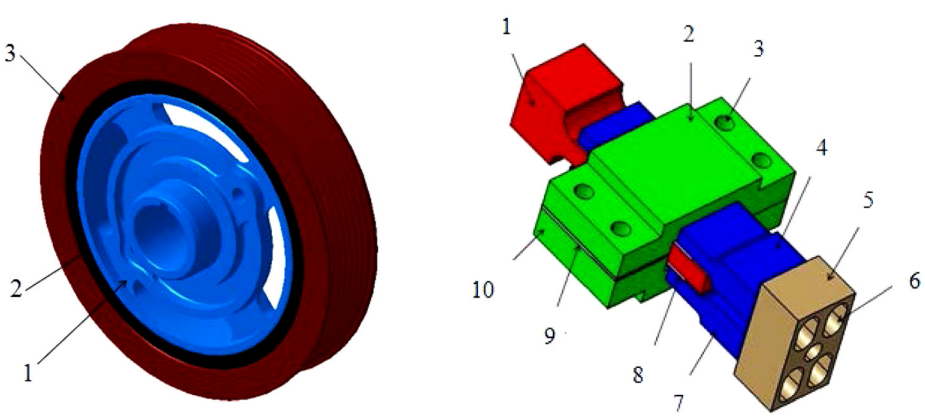

Fig. 1 (*a*) Rubber-damped TVA for an engine crankshaft and (*b*) fixture for measuring shear properties of a rubber specimen (1-moveable block; 2,10-clamping plates; 2,6-fastening bolts; 4,7-locking blocks; 5-intermediate block; 8-rubber specimens; 9-gaskets)

Table 1 Rubber specimen material property and dimensions

Material	Shore hardness/HA	Thickness d_0 (mm)	Area A_0 (mm^2)
EPDM	70	8	40×20

force–displacement relationships during loading and unloading under different compression ratios. For this purpose, a harmonic displacement is applied to the movable block, while the resulting reaction force is measured at the fixed end. In the static experiment, a 5-mm amplitude excitation is applied at a low frequency of 0.2 Hz so as to minimize the viscous force contributions. The dynamic properties of the rubber specimen are obtained under a low amplitude (0.1 mm) excitation with frequency swept from 5 to 500 Hz. The low amplitude excitation is chosen so as to minimize the hysteresis effect attributed to friction between the molecules in the rubber specimen. The measured data are used to determine dynamic stiffness and loss angle of the rubber specimen. The experimental and the data analysis methods for obtaining dynamic stiffness are presented in detail in Ref. [22].

Both the static and dynamic experiments were conducted for different compression ratios ranging from 20% to 50%, which correspond to the variations encountered for rubber rings in TVAs [1]. Figure 2(*a*) illustrates the static force–displacement characteristics of the rubber specimen under different compression ratios, while the dynamic stiffness characteristics of the specimen obtained for different compression ratios in the 5–500 Hz frequency range are presented in Fig. 2(*b*).

2.2 Models and Characterization of Rubber Specimens. The measured data reveal three distinct features of the rubber specimen, namely, the elastic, visco-elastic, and hysteresis effects, as expected. A number of models have been reported to describe these features [13–16]. In this study, three different models, namely, the Kelvin–Voigt, the Maxwell, and the fractional derivative models (Fig. 3) are considered and discussed in view of their ability to describe both the static and dynamic properties of rubber.

In the Kelvin–Voigt model, shown in Fig. 3(*a*), the dynamic stiffness k^* of the rubber specimen can be derived and is given by

$$|k^*| = \sqrt{K_{\mathrm{KV}}^2 + (\omega C_{\mathrm{KV}})^2} \tag{1}$$

where K_{KV} and C_{KV} are the stiffness and shear damping constants, respectively, and ω is the excitation frequency. The above model is considered valid when the contributions due to hysteresis or friction element can be ignored.

Similarly, assuming negligible contributions due to friction element, the dynamic stiffness of the Maxwell model, shown in Fig. 3(*b*), can be given by

$$|k^*| = \sqrt{\left(\frac{\omega^2 C_{\mathrm{Mv}}^2 K_{\mathrm{Mv}}}{K_{\mathrm{Mv}}^2 + \omega^2 C_{\mathrm{Mv}}^2} + K_e\right)^2 + \left(\frac{\omega C_{\mathrm{Mv}} K_{\mathrm{Mv}}^2}{K_{\mathrm{Mv}}^2 + \omega^2 C_{\mathrm{Mv}}^2}\right)^2} \tag{2}$$

where K_{Mv} and C_{Mv} are shear stiffness and shear damping coefficients, respectively, and K_e is the elastic stiffness.

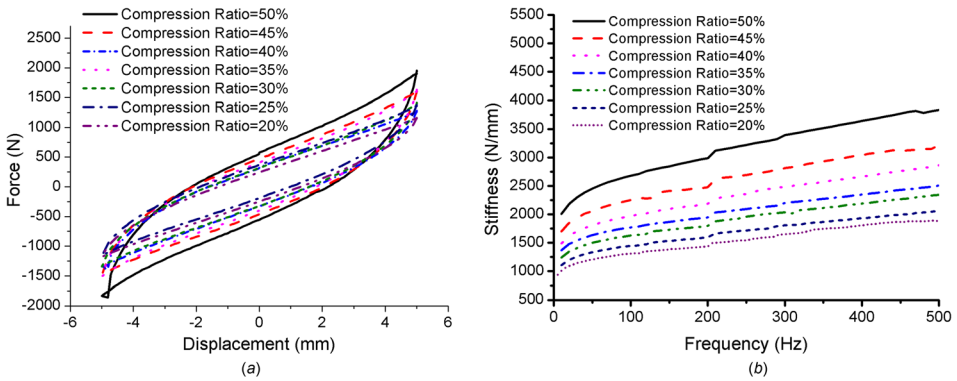

Fig. 2 Measured characteristics of the rubber specimen under different compression ratios: (*a*) force–displacement (excitation amplitude: 5 mm; frequency: 0.2 Hz) and (*b*) dynamic stiffness (excitation amplitude: 0.1 mm)

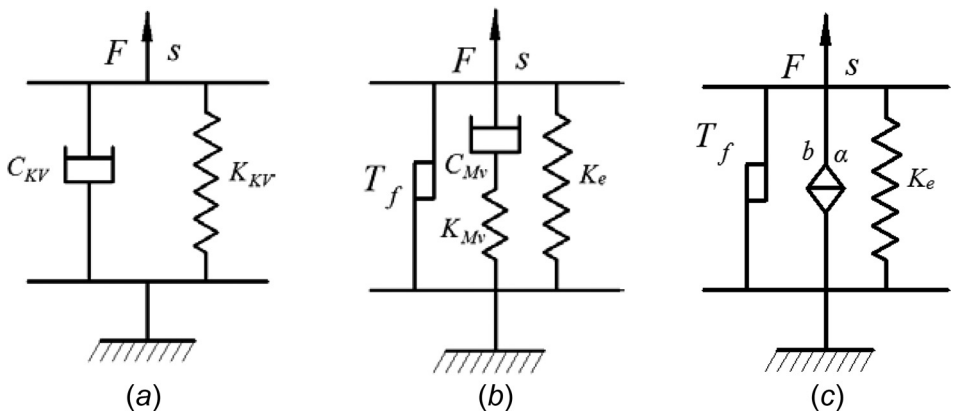

Fig. 3 Models for the rubber specimen (*a*) Kelvin–Voigt model, (*b*) Maxwell model, and (*c*) fractional derivative model

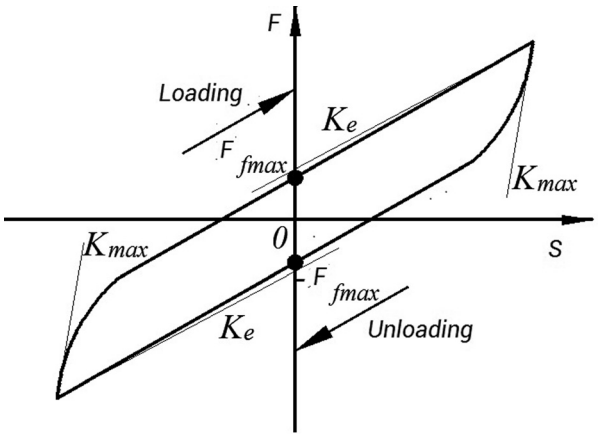

Fig. 4 Typical force–displacement characteristics of a rubber subject to large magnitude deformation at a slow rate

The fractional derivative model, shown in Fig 3(*c*), yields dynamic stiffness of the form [11]

$$|k^*| = |K_e + b(i\omega)^{\alpha}| \tag{3}$$

where constant b and exponent α are the model parameters. The parameters of the models in Eqs. (1)–(3) are identified from the measured dynamic stiffness of the rubber specimen through minimization of error between the model and measured dynamic stiffness.

Under large magnitude deformations applied at a very low speed (in the order of 20 mm per minute), the force–displacement curves obtained during loading and unloading are not coincident for rubber materials, which is evident from the measured static properties of the specimen presented in Fig. 2(*a*). The typical force–displacement properties, shown in Fig. 4, invariably exhibit hysteresis effect. The force versus displacement relations for the rubber specimens are thus described by the friction element, T_f, in the Maxwell and fractional derivate models [16].

Referring to Fig. 4, the force developed during loading F_f can be expressed as [16]

$$F_f = F_{\text{fs}} + \frac{S - S_s}{S_{1/2}(1-\mu) + (S - S_s)}(F_{f\max} - F_{\text{fs}}) \tag{4}$$

where $F_{f\max}$ is the maximum friction force, F_{fs} and S_s are unknown force and displacement, respectively, of the rubber specimen and μ is an intermediate parameter. $S_{1/2}$ is the displacement when force equals half of the maximum friction force, and is given by

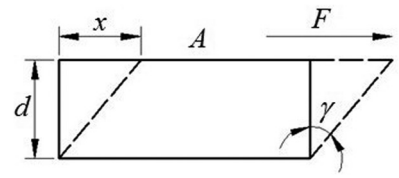

Fig. 6 Deformation of the rubber specimen under a shear load

$$S_{1/2} + \frac{F_{f\max}}{K_{\max} - K_e}; \quad \mu = F_{\text{fs}}/F_{f\max} \tag{5}$$

Similarly, the force developed during unloading is expressed as [16]

$$F_f = F_{\text{fs}} + \frac{S - S_s}{S_{1/2}(1+\mu) - (S - S_s)}(F_{f\max} + F_{\text{fs}}) \tag{6}$$

2.3 Constitutive Models and Parameters Identification. The stiffness and damping properties of a rubber ring are known to depend on its dimensions and compression ratio apart from the rubber compound. In order to account for the dimension dependence of the parameters for modeling shear dynamic properties of rubbers, three constitutive models based on the above-mentioned Kelvin–Voigt, Maxwell, and friction derivative models are formulated as shown in Fig. 5. The relation between the shear stress (τ) and shear strain (γ) in the constitutive models is governed by the constitutive constants. In the Kelvin–Voigt model, the constitutive constants G_{KV} and η_{KV} represent the elastic and viscous damping of the rubber material, respectively. The constitutive constants in the Maxwell model are G_e, G_{MV}, η_{MV}, $\tau_{f\max}$, and $\gamma_{1/2}$. The G_e represents the elastic modulus corresponding to stiffness K_e in Fig. 3(*b*); the G_{MV} and η_{MV} represent the elastics and viscous damping moduli and corresponding to the visco-elastic element in Fig. 3(*b*) characterized by K_{Mv} and C_{Mv}, respectively, and $\tau_{f\max}$ and $\gamma_{1/2}$ represent maximum friction stress and shear strain corresponding to half the maximum friction stress and corresponding to by T_f in Fig. 3(*c*), respectively.

The elastic shear modulus of a rubber specimen subject to shear deformation, shown in Fig. 6, is related to its stiffness and the dimensions such that

$$G = \frac{\tau}{\gamma} = \frac{F/2A}{x/d} = \frac{Fd}{2Ax} = \frac{Kd}{2A} \tag{7}$$

where F is the applied shear force, A is contact area of the compressed rubber specimen with the fixture, x is shear displacement,

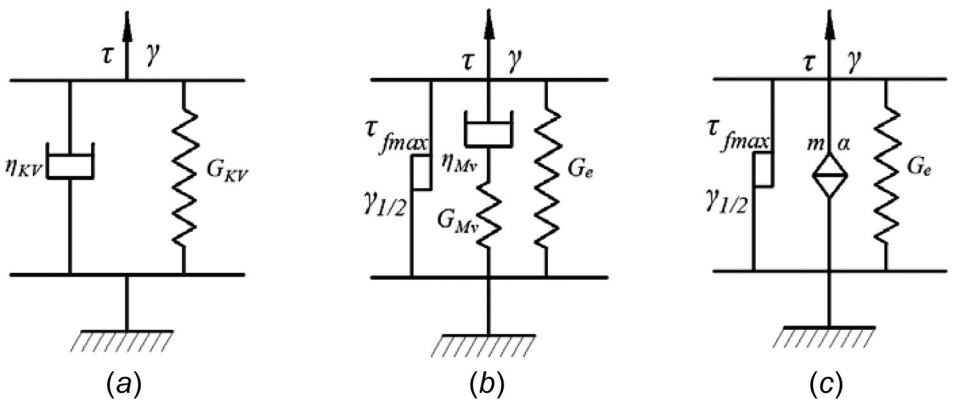

Fig. 5 Constitutive models for describing shear dynamic properties of rubbers based on: (*a*) Kelvin–Voigt model, (*b*) Maxwell model, and (*c*) Fractional derivative model

and d is thickness of the compressed rubber specimen. τ and γ are elastic shear stress and shear strain of the rubber specimen, respectively, and K is its stiffness. In the above equation, the shear stress is obtained from $F/2A$, since two rubber specimens were subject to shear simultaneously in the experiments.

The compression ratio of the rubber specimen ξ is defined as

$$\xi = \frac{d_0 - d}{d_0} \tag{8}$$

Considering the rubber specimen to be incompressible yields

$$A_0 d_0 = Ad \tag{9}$$

where A_0 is the contact area between the fixture and rubber specimen prior to the specimens deformation.

Upon substituting for A and d from Eqs. (8) and (9) into Eq. (7), the elastic shear modulus can be expressed in terms of the compression ratio

$$G = \frac{Kd_0(1-\xi)^2}{2A_0} \tag{10}$$

In a similar manner, the constitutive constant η related to the viscous effect can also be related to the compression ratio as

$$\eta = \frac{Cd_0(1-\xi)^2}{2A_0} \tag{11}$$

where C is the damping coefficient of the rubber specimen.

The maximum shear stress $\tau_{f\max}$ and shear strain $\gamma_{1/2}$ corresponding to half of the maximum shear stress in the constitutive models are obtained in terms of the compression ratio from

$$\tau_{f\max} = \frac{F_{f\max}}{A} = \frac{F_{f\max}(1-\xi)}{A_0} \tag{12}$$

$$\gamma_{1/2} = \frac{x_{1/2}}{d} = \frac{x_{1/2}}{d_0(1-\xi)} \tag{13}$$

In the above relations, $x_{1/2}$ represents the shear deformation corresponding to half of the maximum force $F_{f\max}$ [16].

The fractional derivative constitutive model for the rubber specimen subject to shear deformation, shown in Fig. 6, yields following relations for the visco-elastic shear force F_v and shear stress τ_v

$$F_v = bD^{\alpha}x; \quad \tau_v = mD^{\alpha}\gamma \tag{14}$$

where D is fractional derivative, b is termed as visco-elastic coefficient, and m is the fractional derivative constitutive model parameter. Considering that $\tau_v = F_v/2A$ and $\gamma = x/d$, the parameter m is obtained in terms of the compression ratio and specimen dimensions as

$$m = \frac{bd_0(1-\xi)^2}{2A_0} \tag{15}$$

It should be noted that the parameters G and η in Eqs. (10) and (11) represent the constitutive constants G_{KV} and η_{KV} in the Kelvin–Voigt constitutive model when $K = K_{KV}$ and $C = C_{KV}$ in Fig 3(*a*). Similarly, in the case of the Maxwell constitutive model, the constitutive constant parameters G_{Mv} and η_{Mv} can be described by G and η, respectively, for $K = K_{Mv}$ and $C = C_{Mv}$ in Fig. 3(*b*). The parameter G in Eq. (10) also describes the elastic constitutive constant G_e in the Maxwell and fractional derivative constitutive models, shown in Figs. 5(*b*) and 5(*c*), when $K = K_e$ in the Maxwell and fractional derivative models shown in Figs. 3(*b*) and 3(*c*). The maximum shear stress $\tau_{f\max}$ and shear strain $\gamma_{1/2}$ in Eqs. (12) and (13) are parameters in the Maxwell and fractional derivative constitutive models, shown in Figs. 5(*b*) and 5(*c*).

The parameters of the constitutive models are identified using the measured dynamic shear stiffness of the rubber specimen, presented in Sec. 2.1. These include the elastic shear modulus (G_{KV}) and viscous damping coefficient (η_{KV}) in the Kelvin–Voigt constitutive model, the shear modulus (G_{Mv}) and damping coefficient (η_{Mv}) in the viscos-elastic element of Maxwell constitutive model, and the damping coefficient (m) and the exponent (α) in the fractional derivative constitutive model. Elastic shear modulus (G_e), maximum friction stress ($\tau_{f\max}$), and the shear strain ($\gamma_{1/2}$) in the Maxwell and fractional derivative constitutive models are identified from the measured force–displacement characteristics of the rubber specimen in the quasistatic state considering different compression ratios.

2.3.1 Parameters for Kelvin–Voigt Constitutive Model. The stiffness K_{KV} and damping C_{KV} constants used to define the dynamic stiffness k^* of the Kelvin–Voigt model in Eq. (1) are identified from the measured dynamic stiffness over the 5–500 Hz frequency range for different compression ratios. The method of least squared error minimization is used so as to minimize the error between the computed and measured dynamic stiffness in the above-stated frequency range for the given compression ratio. As an example, Fig. 7 illustrates comparisons of the measured and computed dynamic stiffness considering compression ratio of 50% and 0.1 mm excitation amplitude. The comparison suggests good agreement between the dynamic stiffness obtained from the identified model and the measured data in the chosen frequency range, with the exception of notable deviation at frequencies below 50 Hz. The correlation coefficient (r^2) of the fitted dynamic stiffness model is nearly 0.88, and the estimated K_{KV} and C_{KV} equal to 2601 N/mm and 1.011 Ns/mm, respectively. The results obtained for different compression ratios, however, revealed decreasing stiffness and damping constants with decreasing compression ratio, as seen in Table 2.

The identified model constants can be applied to determine the dynamic stiffness of the specimen for the given compression ratio using Eq. (1). The parameters of the Kelvin–Voigt constitutive model, G_{KV} and η_{KV}, for the given compression ratio can be subsequently obtained from Eqs. (10) and (11) by letting $K = K_{KV}$ and $C = C_{KV}$. Table 2 presents variations in the constitutive model parameters, G_{KV} and η_{KV}, with compression ratio. The results suggest that G_{KV} varies nearly linearly with the compression ratio ($r^2 = 0.973$), while the variations in η_{KV} can be described by a polynomial function in ξ ($r^2 = 0.98$) such that

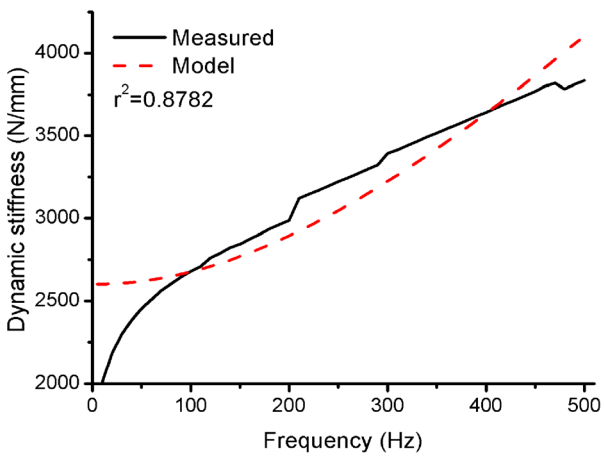

Fig. 7 Comparison of dynamic shear stiffness obtained from the identified Kelvin–Voigt model with the measured data of the rubber specimen (compression ratio: 50%; Excitation amplitude: 0.1 mm)

Table 2 Identified parameters of the Kelvin–Voigt and Kelvin–Voigt constitutive models of the rubber specimen corresponding to different compression ratios

Compression ratio ξ (%)	Shear stiffness K_{KV} (N/mm)	Shear damping C_{KV} (Ns/mm)	Elastic shear modulus G_{KV} (MPa)	Viscous damping coefficient η_{KV} (MPa · s)
20	1303	0.3811	4.1696	0.001220
25	1406	0.5275	3.9544	0.001484
30	1581	0.6053	3.8734	0.001483
35	1722	0.6366	3.6377	0.001345
40	1912	0.7422	3.4416	0.001336
45	2147	0.8949	3.2473	0.001354
50	2601	1.0110	3.2513	0.001264

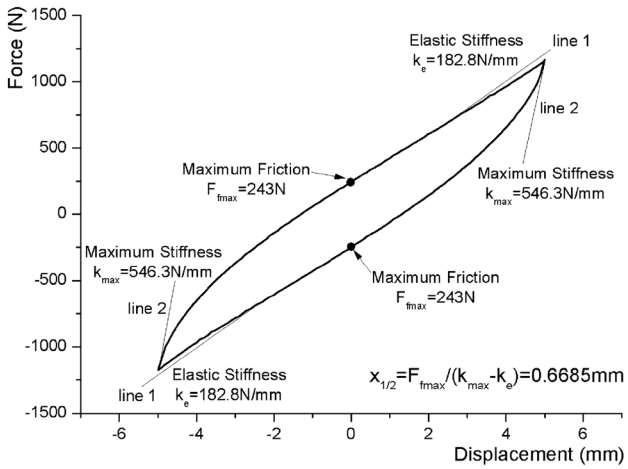

Fig. 8 Identifications of elastic stiffness ke, maximum friction force F_{fmax}, and displacement × 1/2 corresponding to half the maximum friction force from the measured force–displacement characteristics of the rubber specimen under 20% compression ratio

$$G_{\mathrm{KV}} = -3.286\xi + 4.804 \tag{16}$$

$$\eta_{\mathrm{KV}} = 9 * 10^{-9}\xi^4 + 1 * 10^{-6}\xi^3 - 7 * 10^{-5}\xi^2 + 0.0017\xi - 0.0132 \tag{17}$$

2.3.2 Parameters for Elastic and Fractional Elements of the Maxwell and Fractional Derivative Constitutive Models. As seen in Figs. 5(*b*) and 5(*c*), both the Maxwell and fractional derivative constitutive models include the elastic and friction elements. The elastic modulus and friction parameters for each of the model corresponding to a given compression ratio could be identified directly from the measured static force–displacement characteristics during loading as well as unloading. As an example, Fig. 8 illustrates the measured force–displacement property of rubber specimen under compression ratio of 20%. The maximum friction force $F_{f\max}$ is identified as the force corresponding to zero displacement, while the elastic stiffness k_e and the maximum stiffness $k_{\max}$ are obtained from slopes of lines 1 and 2, respectively. The displacement $x_{1/2}$ corresponding to half of $F_{f\max}$ is obtained from

$$x_{1/2} = \frac{F_{f\max}}{k_{\max} - k_e} \tag{18}$$

The elastic and friction element parameters identified for 20% compression ratio are also illustrated in Fig. 8. The elastic modulus G_e, the maximum friction stress $\tau_{f\max}$, and the shear strain $\gamma_{1/2}$ corresponding to half of maximum friction stress are subsequently obtained from Eqs. (10), (12), and (13), respectively. Table 3 summarizes these computed parameters of the Maxwell and fractional derivative constitutive models together with the elastic and friction element parameters for different compression ratios. The results clearly show strong dependence of the constitutive model parameters on the compression ratio. It is further seen that the elastic shear modulus G_e and maximum friction stress $\tau_{f\max}$ decrease and increase, respectively, with increasing compression ratio in a nearly linearly manner. The least square error minimization method is used to obtain following relations for G_e, $\tau_{f\max}$, and $\gamma_{1/2}$ with the compression ratio:

$$G_e = -1.008\xi + 0.776, \quad r^2 = 0.9759 \tag{19}$$

$$\tau_{f\max} = 0.173\xi + 0.0868, \quad r^2 = 0.9534 \tag{20}$$

$$\gamma_{1/2} = \frac{0.0759}{1 - \xi}, \quad r^2 = 0.8859 \tag{21}$$

2.3.3 Parameters for Visco-Elastic Element of the Maxwell Constitutive Model. In the Maxwell model, the dynamic stiffness of the rubber specimen is related to the shear stiffness and damping coefficients, K_{MV} and C_{MV}, as seen in Eq. (2). Measured

Table 3 Identified elastic and friction elements parameters of the Maxwell and fractional derivative constitutive models of the rubber specimen corresponding to different compression ratios

	Maxwell model			Maxwell constitutive model		
Compression ratio ξ (%)	Elastic stiffness k_e (N/mm)	Maximum friction $F_{f\max}$ (N)	Displacement at half of $F_{f\max}$ $x_{1/2}$ (mm)	Elastic shear modulus G_e (MPa)	Maximum friction stress $\tau_{f\max}$ (MPa)	Strain at the half of $\tau_{f\max}$, $\gamma_{1/2}$
20	182.8	243	0.6685	0.5850	0.1215	0.104453
25	186.6	279	0.5915	0.5248	0.1308	0.098583
30	193.5	321	0.5608	0.4741	0.1404	0.100143
35	195.0	365	0.5576	0.4119	0.1483	0.107231
40	206.0	402	0.6045	0.3708	0.1508	0.125938
45	196.1	463	0.6010	0.2966	0.1592	0.136591
50	241.0	575	0.6686	0.3013	0.1797	0.16715

Table 4 Identified visco-elastic element parameters of the Maxwell and Maxwell constitutive models

	Maxwell model		Maxwell constitutive model	
Compression ratio ξ (%)	Visco-elastic stiffness K_{Mv} (N/mm)	Shear damping C_{Mv} (Ns/mm)	Visco-elastic shear modulus G_{Mv} (MPa)	Visco-elastic damping Coefficient η_{Mv} (MPa · s)
20	1340	5.950	4.2880	0.019040
25	1608	6.707	4.5225	0.018863
30	1852	7.293	4.5374	0.017868
35	1991	8.736	4.2060	0.018455
40	2297	9.051	4.1346	0.016292
45	2684	9.432	4.0596	0.014266
50	3197	11.98	3.9963	0.014975

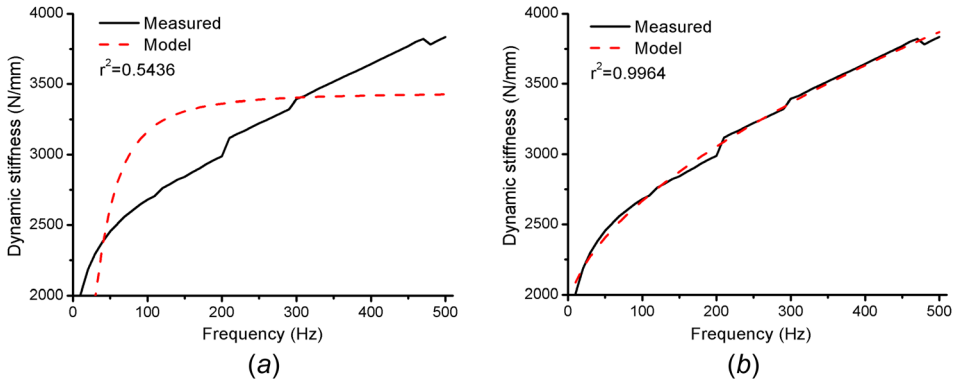

Fig. 9 Comparisons of estimated dynamic shear stiffness of the rubber specimen with the measured data: (*a*) Maxwell constitutive model and (*b*) fractional derivative constitute model (compression ratio: 50%, excitation amplitude: 0.1 mm)

dynamic stiffness data of the specimen in the 5–500 Hz frequency range are used to determine these parameters using the least squares method corresponding to each compression ratio of the specimen. The two constitute model parameters, G_{Mv} and η_{Mv}, are subsequently obtained from Eqs. (10) and (11), respectively. Table 4 summarizes the identified parameters and the computed constitutive model parameters corresponding to different compression ratios. It is evident that the visco-elastic element model parameters are strongly dependent on the compression ratio. Least squares error minimization method is further used to identify following relations for the visco-elastic shear modulus (G_{Mv}) and visco-elastic damping coefficient (η_{Mv}) with the compression ratio (ξ) as

$$G_{\mathrm{Mv}} = 127.6\xi^3 - 140.7\xi^2 + 47.8\xi - 0.648, \quad r^2 = 0.92 \quad (22)$$

$$\eta_{\mathrm{Mv}} = 0.468\xi^3 - 0.522\xi^2 + 0.168\xi + 0.0023, \quad r^2 = 0.89 \quad (23)$$

The identified stiffness and damping coefficients of the Maxwell model are used to estimate dynamic stiffness of the specimen in the entire frequency range. As an example, Fig. 9(*a*) presents comparison of the estimated dynamic stiffness with the measured data corresponding to 50% compression ratio and 0.1 mm excitation. The results show poor agreement between the estimated and measured dynamic stiffness in the entire frequency range ($r^2 = 0.544$). The dynamic stiffness of the Maxwell model tends to saturate at higher frequencies, as it is evident from Eq. (2), while the measured stiffness suggests nearly linear increase with frequency at frequencies above 200 Hz.

2.3.4 Parameters for Visco-Elastic Element of the Fractional Derivative Constitutive Model. In the fractional derivative model, the dynamic stiffness of the rubber specimen is related to model constants, b and α, as seen in Eq. (3). Measured dynamic stiffness data of the specimen in the 5–500 Hz frequency range are used to determine these model constants corresponding to each compression ratio. The constitutive model parameters, m, is subsequently obtained from Eq. (13) for each compression ratio. Table 5 summarizes the identified parameters of the fractional derivative model (b, α) and the computed constitutive model parameter (m) corresponding to different compression ratios. The results suggest that the exponent α of the fractional derivative model remains nearly constant in the range of compression ratios considered (mean = 0.545; standard deviation = 0.013), while the coefficients b and m generally increase in quadratic and linear manners, respectively, with compression ratio. The least squares error minimization method is used to identify following relations between the parameters b and m and the compression ratio (ξ):

$$b = 0.0223\xi^2 - 0.6523\xi + 17.824, \quad r^2 = 0.998 \quad (24)$$

$$m = 0.0294\xi + 0.0369, \quad r^2 = 0.862 \quad (25)$$

As an example, Fig. 9(*b*) presents comparison of the dynamic stiffness estimated from the identified model with the measured data in the 5–500 Hz frequency range considering 50% compression ratio and 0.1 mm excitation amplitude. The comparison suggests very good agreement between the estimated and measured dynamic stiffness in the entire frequency range ($r^2 = 0.996$). Similar degree of agreement was also observed for different compression ratios. From the results presented in Figs. 7 and 9, it is deduced that the fractional derivative model can accurately describe the variations in dynamic stiffness of the rubber specimens in the range of compression ratios considered in the study.

3 Measurements and Estimations of the Natural Frequency of a Rubber-Damped TVA

3.1 Measurements of Natural Frequency. An experimental setup is designed and developed for measuring natural frequency

Table 5 Identified visco-elastic element parameters of the fractional derivative models

	Fractional derivative model		Fractional derivative constitutive model
Compression ratio ξ /%	b/(Ns$^{\alpha}$/mm)	α	m /(Ns$^{\alpha}$/mm^3)
20	13.821	0.5450	0.04423
25	14.816	0.5489	0.04167
30	19.012	0.5525	0.04658
35	22.347	0.5469	0.04721
40	27.116	0.5524	0.04881
45	33.342	0.5529	0.05043
50	41.088	0.5172	0.05136

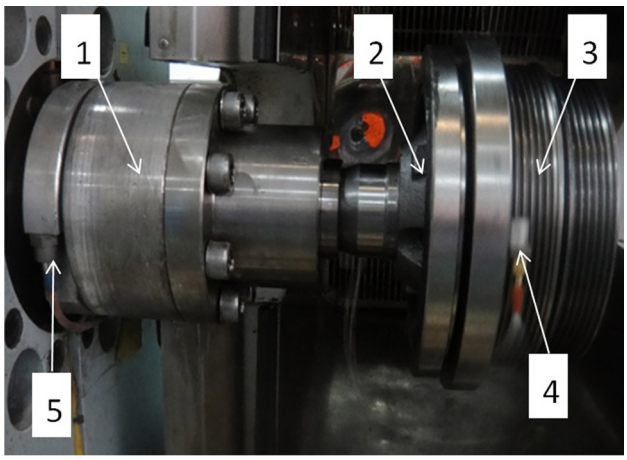

Fig. 10 Experimental setup for measurements of frequency response function (FRF) of the rubber-damped TVA (1-excitation shaft; 2-hub; 3-inertia ring; 4,5-accelerometers)

of the rubber-damped TVA over a range of excitation magnitudes. A pictorial view of the experimental setup is illustrated in Fig. 10, where the hub of the TVA is connected to an excitation shaft, while the inertia ring is in a free state. The shaft can generate different magnitudes of oscillatory angular motions over a wide frequency range. The experiment was designed to measure FRF of the TVA under different excitation magnitudes in the 100–400 Hz frequency range, while the compression ratio of the inner ring was limited to 40%. For this purpose, two accelerometers were installed to measure accelerations due to excitation of the shaft and that due to motion transmitted to the inertia ring, as shown in Fig. 10. The FRF of the TVA under different excitations were subsequently obtained from the ratio of Fourier transform of acceleration at the inertia ring to that of the hub and expressed in terms of both the magnitude ratio and the phase. The frequency corresponding to the peak magnitude ratio is considered as the natural frequency of the TVA for the given oscillatory excitation amplitude.

As an example, Fig. 11(*a*) illustrates the measured magnitude ratio and phase response of the TVA under 0.01 deg oscillation amplitude and rubber ring compression ratio of 40%. The magnitude ratio approaches the peak value near 360 Hz. The phase angle near this frequency is close to −90 deg. This frequency can thus be considered as the natural frequency of the rubber-damped TVA. However, the FRF of the TVA and thus the natural frequency is strongly influenced by the oscillations amplitude, due to strong and nonlinear dependence of the dynamic stiffness and damping of the rubber ring on the excitation magnitude [25,26]. The measurements were thus repeated under different amplitudes of oscillations, ranging from 0.01 deg to 0.07 deg, and the magnitude ratio responses of the TVA are presented in Fig. 11(*b*). The results clearly show that the frequency corresponding to peak magnitude ratio decreases as the oscillation angle amplitude is increased. This is attributed to special character of the elastomers, namely, the reductions in effective dynamic stiffness with increasing deformation [26]. Considering the observed variations in frequency corresponding to peak magnitude ratio, it is considered more appropriate to refer to this frequency as the nonlinear natural frequency of the rubber-damped TVA.

3.2 Modeling a Rubber-Damped TVA. The natural frequency of the TVA may be estimated from the stiffness of the rubber ring and the MOI of the inertia ring. Owing to strong

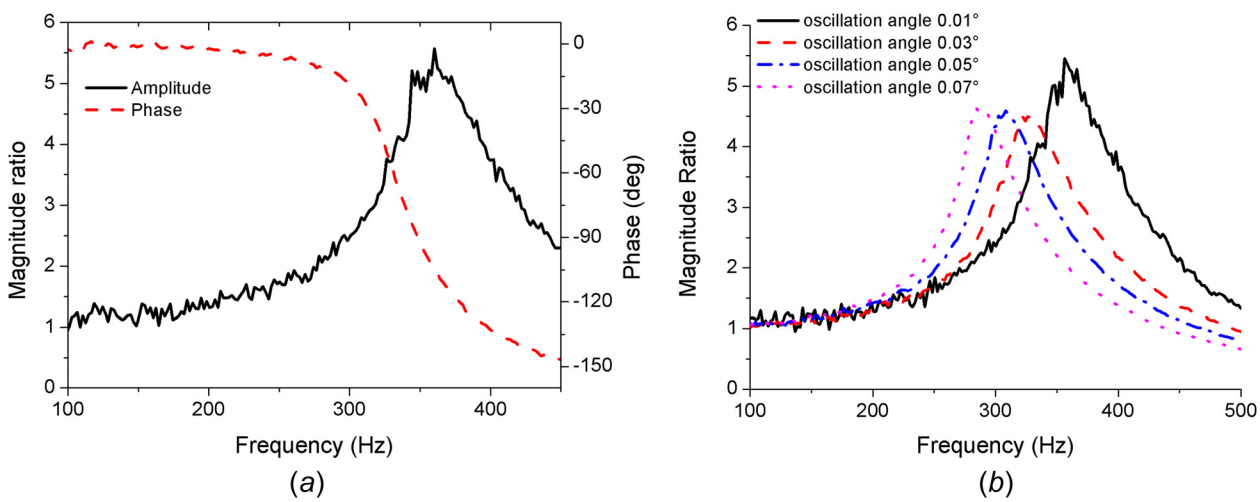

Fig. 11 Measured frequency response characteristics of the TVA: (*a*) magnitude ratio and phase responses under 0.01 deg oscillation angle amplitude and (*b*) magnitude ratio under different oscillation angle amplitudes

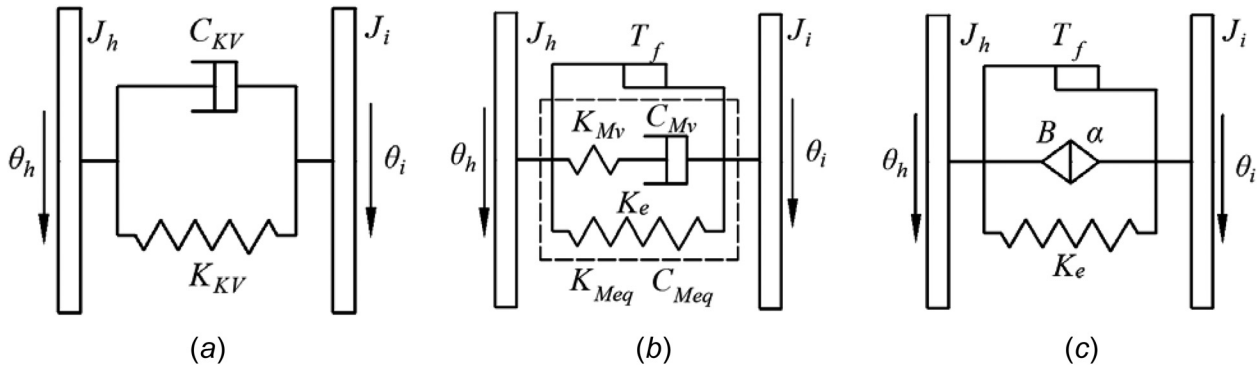

Fig. 12 TVA model employing different models of the rubber ring: (*a*) Kelvin–Voigt model, (*b*) Maxwell model, and (*c*) fractional derivative model

dependency of the dynamic stiffness and damping property of the rubber on the excitation amplitude, the characterization of rubber ring stiffness poses considerable complexity. In this study, the stiffness of the rubber ring is obtained from the properties of the rubber specimen measured and modeled in Sec. 2 considering different models. For this purpose, the models of rubber-damped TVAs are first developed using the Kelvin–Voigt, Maxwell, and fractional derivative models of the rubber specimen, as shown in Fig. 12. In the models, J_h and J_i represent the mass MOI due to hub and the inertia ring, respectively, θ_h is the oscillation angle excitation applied to the hub, and θ_i is the response of the inertia ring. The dynamic characteristics of the rubber ring in the TVA model are described using the rubber specimen models presented in Fig. 3, which are further explained below.

In the Kelvin–Voigt model, shown in Fig. 12(*a*), the rubber ring is represented by a constant torsional stiffness (K_{KV}) and torsional damping coefficient (C_{KV}). The differential equation of motion for the inertia ring is thus expressed as

$$J_i\ddot{\theta}_i = K_{\mathrm{KV}}(\theta_h - \theta_i) + C_{\mathrm{KV}}\left(\dot{\theta}_h - \dot{\theta}_i\right) \tag{26}$$

In the Maxwell model used for describing the rubber ring, shown in Fig. 12(*b*), the torque developed by the rubber ring is divided into three components, namely, the elastic torque, the visco-elastic torque, and the friction torque. These can be, respectively, obtained from the elastic torsional stiffness (K_e), the visco-elastic stiffness (K_{Mv}), the damping coefficient (C_{Mv}), and the friction torque (T_f), as described in Secs. 2.2 and 2.3. The equivalent torsional stiffness (K_{Meq}) and the damping coefficients (C_{Meq}) are derived from the elastic stiffness, visco-elastic stiffness, and damping and are expressed as

$$K_{\mathrm{Meq}} = \frac{\omega^2 C_{\mathrm{Mv}}^2 K_{\mathrm{Mv}}}{K_{\mathrm{Mv}}^2 + \omega^2 C_{\mathrm{Mv}}^2} + K_e \quad C_{\mathrm{Meq}} = \frac{C_{\mathrm{Mv}} K_{\mathrm{Mv}}^2}{K_{\mathrm{Mv}}^2 + \omega^2 C_{\mathrm{Mv}}^2} \tag{27}$$

The differential equation of motion for the inertia ring is subsequently obtained considering the equivalent stiffness and damping properties in addition to the friction torque such that

$$J_i\ddot{\theta}_i = K_{\mathrm{Meq}}(\theta_h - \theta_i) + C_{\mathrm{Meq}}\left(\dot{\theta}_h - \dot{\theta}_i\right) + T_f \tag{28}$$

The T_f in Eq. (28) is friction torque and the relation between the friction torque and angle is the same as that shown in Fig. 4.

In the fractional derivative model of the TVA, shown in Fig. 12(*c*), the torque developed by the rubber ring is also divided into three components, as in the case of the Maxwell model. While the elastic and friction torque components are identical to those obtained for the Maxwell model, the visco-elastic torque is defined as a function of the inner ring deformation, as described in Eq. (14) [18]

$$T_v = BD^{\alpha}(\theta_h - \theta_i) \tag{29}$$

In the above relation, B is a coefficient, exponent α is the order of fractional derivative that ranges from 0 to 1, and $D^{\alpha}(\bullet)$ represents the time derivative of function $(\bullet)$ of order α. The differential equation of motion for the inertia ring is subsequently obtained as

$$J_i\ddot{\theta}_i = K_e(\theta_h - \theta_i) + BD^{\alpha}(\theta_h - \theta_i) + T_f \tag{30}$$

3.3 Estimations of the Natural Frequency of a Rubber-Damped TVAs. For a rubber-damped TVA with an irregular shape of the hub, as shown in Fig. 13, the torsional stiffness K can be determined from [25]

$$K = 4\pi G \int_0^L \frac{r_1(x)^2 r_2(x)^2}{r_1(x)^2 - r_2(x)^2} dx \tag{31}$$

where $r_1(x)$ and $r_2(x)$ are the outer radius of the hub and inner radius of the inertia ring, respectively, which are function of axial displacement x of the hub. L is width of the rubber ring, which defines the domain of integration. In the above relation, G is shear modulus of the rubber specimen, which represents the shear modulus G_{KV} in the Kelvin–Voigt constitutive model, G_e in the Maxwell and the fractional derivative constitutive models, and G_{Mv} in

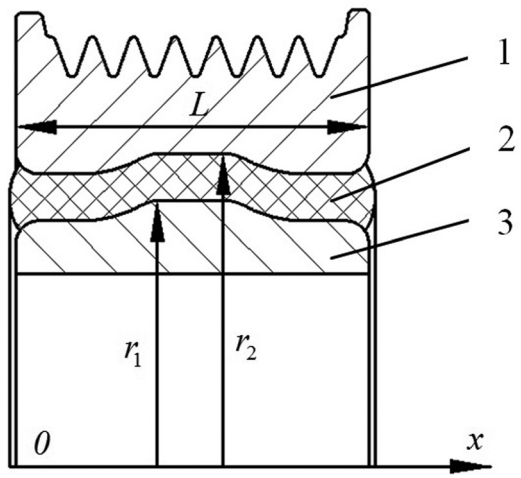

Fig. 13 TVA with an irregularly shaped hub (1-inertia ring; 2-rubber specimen; 3-hub)

the Maxwell constitutive model. Equation (31) can thus be used to determine the elastic stiffness K_e in the Maxwell and fractional derivative models using the shear modulus parameters estimated in Sec. 2.3.

The damping coefficient of the rubber specimen in TVA with an irregularly shaped hub can be obtained from [21]

$$C = 4\pi\eta \int_0^L \frac{r_1(x)^2 r_2(x)^2}{r_1(x)^2 - r_2(x)^2} dx \tag{32}$$

The above equation yields damping constants C_{KV} and C_{Mv} of the Kelvin–Voigt and Maxwell models, respectively, by substituting for η by the estimated constitutive constants η_{KV} and η_{Mv} (Sec. 2.3). For rubber-damped TVAs with a regular shaped hub (cylindrical), the mean of the inner and the outer radii of the rubber ring, $r_{0,}$ is constant. In this case, maximum shear stress ($\tau_{f\max}$) can be related to maximum friction torque ($T_{f\max}$) as:

$$T_{f\max} = \tau_{f\max} \cdot A_c \cdot r_0 = \tau_{f\max} \cdot 2\pi r_0 L \cdot r_0 = 2\pi\tau_{f\max} r_0^2 L \tag{33}$$

where A_c is area of the rubber ring.

For a TVA with irregularly shaped hub (Fig. 13), the relationship between $\tau_{f\max}$ and $T_{f\max}$ is obtained from

$$T_{f\max} = 2\pi\tau_{f\max} \int_0^L r_0(x)^2 dx \tag{34}$$

Solutions of Eqs. (31)–(34) permit the estimations of torsional stiffness and damping provided by the rubber ring of a rubber-damped TVA. The friction torque within the hub and the inertia ring can be further obtained using the constitutive model parameters of the rubber specimen.

3.3.1 Kelvin–Voigt Model. Using the above-estimated stiffness and damping parameters of the Kelvin–Voigt model, the natural frequency of a rubber-damped TVA can be obtained from

$$f_{\mathrm{KV}} = f_{\mathrm{KVn}}\sqrt{1-\zeta^2} = \frac{1}{2\pi}\sqrt{\frac{K_{\mathrm{KV}}}{J_i}\left(1 - \frac{C_{\mathrm{KV}}^2}{4K_{\mathrm{KV}}J_i}\right)} \tag{35}$$

where f_{KVn} is the undamped natural frequency of a rubber-damped TVA obtained from the Kelvin–Voigt model and ζ is the damping ratio. From the above relation, it is evident that the natural frequency of the TVA remains constant, irrespective of the excitation magnitude and frequency.

3.3.2 Maxwell Model. From the equation of motion of the inertia ring based upon the Maxwell model of the rubber ring, Eq. (28), it is evident that the equivalent stiffness and damping coefficients (K_{Meq} and C_{Meq}) are dependent on the excitation frequency, as seen in Eq. (27). Furthermore, the friction torque (T_f) is dependent on the excitation amplitude. The natural frequency of the TVA thus cannot be obtained directly from Eq. (28). Equation (28), however, can be numerically solved for the frequency response characteristics of the TVA under constant amplitude angular excitation of the hub. The natural frequency for a given excitation amplitude is then estimated as the frequency corresponding to peak magnitude ratio $|\theta_i/\theta_h(\omega)|$. As an example, Fig. 14 illustrates the magnitude ratio response of the TVA model employing Maxwell model of the rubber ring considering 40% compression ratio of the rubber ring and 0.01 deg angular excitation amplitude applied to the hub. The frequency response reveals peak magnitude ratio near 393 Hz, which is considered as the natural frequency of the TVA for the given compression ratio and excitation amplitude. The dependence of the natural frequency of the TVA on the excitation amplitude is further obtained through repeated solutions of Eq. (28) under different amplitudes of excitation. The results are discussed in Sec. 3.3.3.

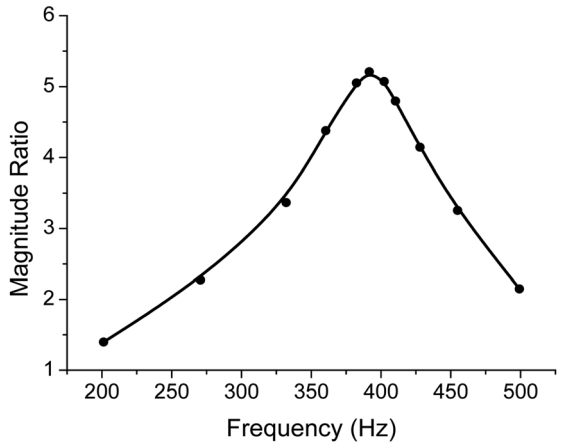

Fig. 14 Frequency response of the rubber-damped TVA employing Maxwell mode of the inertia ring (compression ratio: 40%; excitation amplitude: 0.01 deg)

3.3.3 Fractional Derivative Model. The natural frequency of the rubber-damped TVA model employing fractional derivative model of the rubber ring is estimated using the method described above for the Maxwell model. The nonlinear equation of motion of the inertia ring, Eq. (30), is solved in a similar manner under different amplitudes of excitation. The solutions, however, involved discretization of the visco-elastic moment term, $T_v = BD^{\alpha}(\theta_h - \theta_i)$ in the following manner [17]

$$T_v(n\Delta t) = B\Delta t^{-\alpha}\sum_{j=0}^{n-1}\{A_{j+1}[\theta_h(n\Delta t - j\Delta t) - \theta_i(n\Delta t - j\Delta t)]\} \tag{36}$$

In the above equation, A_{j+1} are the Grunwald factors, given by

$$A_{j+1} = \frac{\Gamma(j-\alpha)}{\Gamma(-\alpha)\Gamma(j+1)} \tag{37}$$

where $\Gamma(\bullet)$ is the Gamma function. The equation of motion, Eq. (30), is subsequently expressed in the discrete form considering the time step Δt as

$$\theta_i(n\Delta t + \Delta t) = \left\{\left(\frac{2J_i}{\Delta t^2} - K_e\right)\theta_i(n\Delta t) - \frac{J_i}{\Delta t^2}\theta_i(n\Delta t - \Delta t) + K_e\theta_h(n\Delta t) + B\Delta t^{-\alpha}\sum_{j=0}^{n-1}\{A_{j+1}[\theta_h(n\Delta t - j\Delta t) - \theta_i(n\Delta t - j\Delta t)]\right\} + T_f(n\Delta t)\Big\}\Big/\left(\frac{J_i}{\Delta t^2}\right) \tag{38}$$

The fractional derivative model parameter B in the above expression is obtained considering the viscous torque and viscous strain relationship. For the TVA with a uniform cylindrical hub, the viscous torque T_v is obtained from the shear force F_v developed along the circumference such that

$$T_v = F_v r_h = \tau_v A r_h \tag{39}$$

where A is the contact area between the rubber ring and the hub and r_h is the inner radius of the rubber ring. Since the mean radius r_0 is significantly greater than the ring thickness, the visco-elastic torque can be expressed as

$$T_v = \tau_v A r_0 \tag{40}$$

Assuming small deformations, the angular deformation of the rubber ring is also related to its tangential displacement x as

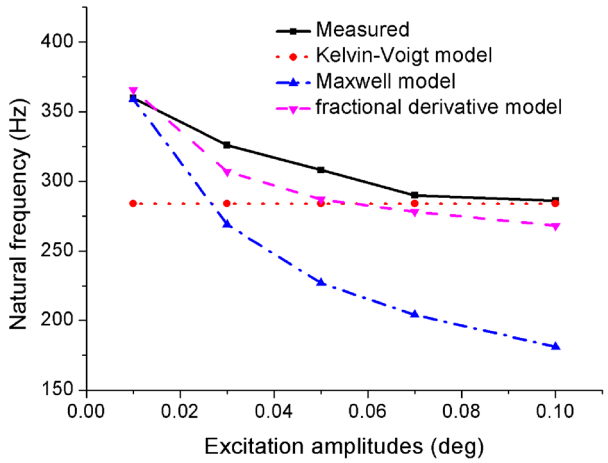

Fig. 15 Comparisons of natural frequencies predicted from the rubber-damped TVA models with those obtained from the measured frequency response characteristics under different excitation amplitudes

$$\Delta\theta = \theta_h - \theta_i = \frac{x}{r_0} \tag{41}$$

The definition of the compression ratio together with incompressibility of the rubber ring, described in Eqs. (8) and (9), yields

$$\xi = \frac{h_0 - h}{h_0} \tag{42}$$

$$2\pi r_0 L_0 \cdot h_0 = 2\pi r_0 L \cdot h \tag{43}$$

where h_0 and h are heights of rubber ring before and after compression, respectively, and L_0 and L are the lengths before and after compression. Considering that $\gamma = x/h$, the shear stress in the fractional derivative constitutive model can be expressed in terms of the lateral displacement as

$$\tau_v = mD^\alpha \frac{x}{h} \tag{44}$$

The above relation together with those for the visco-elastic torque in Eqs. (29) and (40) yields

$$BD^\alpha(\theta_h - \theta_i) = \frac{mAr_0^2 D^\alpha(\theta_h - \theta_i)}{h} \tag{45}$$

The constitutive model constant B is obtained upon simplifying the above relation and substituting for A in terms of compression ratio, $A = 2\pi r_0 L = (2\pi r_0 L_0)/(1-\xi)$, as

$$B = \frac{mAr_0^2}{h} = \frac{2\pi r_0^3 m L_0}{h_0(1-\xi)^2} \tag{46}$$

The computed value of B is used to determine the visco-elastic torque T_v in Eq. (36), and Eq. (38) is subsequently solved for frequency response of the rubber-damped TVA model employing the fractional derivative model of the rubber ring under the given constant excitation magnitude. The geometric parameters of the rubber ring are taken as $r_1 = 47$ mm, $r_2 = 50$ mm, $r_0 = 48.5$ mm, $L_0 = 19.2$ mm, and $h_0 = 5$ mm, while $J_i = 0.0062$ kg/m^2. Figure 14(*b*) illustrates the magnitude ratio response of the TVA model employing the fractional derivative model of the rubber ring considering 40% compression ratio and 0.01 deg angular excitation amplitude. The magnitude ratio approaches the peak value near 366 Hz, which is considered as the natural frequency of the TVA for the given compression ratio and excitation amplitude. The dependence of the natural frequency of the TVA on the excitation amplitude is further obtained through repeated solutions under different amplitudes of excitation. The results are discussed in Section 3.4.

3.4 Comparisons of the Natural Frequency of a Rubber-Damped TVA Estimated From Different Rubber Ring Models. The natural frequency of the rubber-damped TVA model employing different constitutive models of the rubber rings is evaluated under different excitation magnitudes and compared in Fig. 15. The results are obtained considering the above-mentioned geometric parameters of the rubber ring and 40% compression ratio. The figure also presents the natural frequencies estimated from the measured FRF. The relative errors of each constitutive model with respect to the measured frequencies are also summarized in Table 6. The results show that the Kelvin–Voigt model owing to its constant stiffness and damping constants yields constant natural frequency of the TVA for the entire range of excitation magnitudes. The relative error between the model-predicted and measured frequencies, however, decreases with increasing excitation magnitude, suggesting that the constant model parameters could be considered valid only under higher excitation magnitudes.

The Maxwell and fractional derivative models of the rubber ring exhibit decreasing natural frequencies of the TVA with increasing excitation amplitudes. This tendency is also evident from the measured frequencies, as seen in Fig. 15. The Maxwell model, however, exhibits relatively larger deviations from the measured frequencies compared to the fractional derivative model. Moreover, the error between measured and estimated frequencies from the Maxwell model increases substantially with increasing excitation magnitude, and approaches as high as 36.7% under 0.1 deg excitation. This suggests that the Maxwell model could be considered valid under only very small excitation amplitudes. The fractional derivation model provides more effective estimations of the natural frequencies over the entire range of excitation magnitudes considered in the study. The relative error ranges from 1.67% to 6.83% for the entire range of excitations. This is attributed to the fact that the fractional derivative model constant B strongly depends upon the excitation amplitude, as seen in Eq. (46), in addition to the friction torque. The Maxwell model, on the other hand, considers the amplitude dependence of the friction torque alone. From the view point of engineering applications, it can be deduced that the proposed fractional derivative model together with the model parameters identification methods could provide reasonably accurate estimation of natural

Table 6 Relative errors between the calculated and measured natural frequency of a TVA

	Relative error (%)		
Excitation amplitude A_e (deg)	Kelvin–Voigt model	Maxwell model	Fractional derivative model
0.01	21.1	9.2	1.67
0.03	12.9	17.5	5.83
0.05	7.79	22.7	6.83
0.07	2.07	26.3	4.14
0.1	0.70	36.7	6.29

frequencies of a rubber-damped TVA prior to the prototype designs.

4 Conclusions

(1) The study proposed methods for experimental characterizations of shear properties of rubber specimens considering different compression ratios and natural frequencies of a rubber-damped TVA under a range of excitation magnitudes. It is shown that the static and dynamic properties of the rubber material are strongly dependent upon the compression ratio, while the natural frequency of a rubber-damped TVA decreases with increasing excitation magnitude.

(2) It is concluded that the fractional derivative model yields more accurate prediction of dynamic stiffness of the rubber over wide ranges of frequency and compression ratio when compared to the Maxwell and Kelvin–Voigt models. The rubber material models were subsequently used to estimate natural frequency of the TVA comprising the rubber ring, and its dependence upon excitation magnitude and thereby the rubber ring deformation.

(3) It is shown that the Kelvin–Voigt model with constant and excitation-independent stiffness and damping parameters cannot describe the decreasing tendency of natural frequency with increasing excitation magnitude. The natural frequencies estimated from the Maxwell and fractional derivative models revealed this tendency, while the Maxwell model revealed significantly larger deviations from the measured frequencies, especially under higher excitation magnitudes. The fractional derivative model provided more accurate estimations of natural frequencies over the entire range of excitation magnitudes.

(4) It is concluded that the proposed fractional derivative model together with the model parameters identification methods could be used to estimate natural frequency of a TVA before prototype, thus reducing trails and errors for determining natural frequency of a TVA.

Acknowledgment

The authors acknowledge the financial support from the National Natural Science Foundation of China (Grant Nos. 11472107 and 51275175) and Natural Science Foundation of Guangdong (Grant No. 2014A030313254), and experimental supports provided by Ningbo Tuopu Group Co., Ltd., China, especially the technical supports given by Yajie Wan, Junwei Rong, and Xu Zhao.

References

[1] Mendes, A. S., Meirelles, P. S., and Zampieri, D. E., 2008, "Analysis of Torsional Vibration in Internal Combustion Engines: Modeling and Experimental Validation," Inst. Mech. Eng. Part K, **222**(2), pp. 155–178.
[2] Thomson, W. T., 1981, *Theory of Vibration With Applications*, Prentice Hall, Englewood Cliffs, NJ.
[3] Hartog Den, J. P., 1985, *Mechanical Vibrations*, Dover, New York.
[4] Shangguan, W. B., and Pan, X. Y., 2008, "Multi-Mode and Rubber-Damped Torsional Vibration Absorbers for Engine Crankshaft Systems," Int. J. Veh. Des., **47**(1–4), pp. 176–188.
[5] Sommier, E., Fotsing, E. R., Ross, A., and Lavoie, M., 2014, "Characterization of the Injection Molding Process of Passive Vibration Isolators," J. Elastomers Plast., **1**(1), pp. 1–12.
[6] Sun, Y., and Thomas, M., 2011, "Control of Torsional Rotor Vibrations Using an Electrorheological Fluid Dynamic Absorbers," J. Vib. Control, **17**(8), pp. 1253–1264.
[7] Hoang, N., Zhang, N., and Du, H., 2009, "A Dynamic Absorber With a Soft Magnetorheological Elastomer for Powertrain Vibration Suppression," Smart Mat Struct., **18**(7), p. 074009.
[8] Monroe, R. J., and Shaw, S. W., 2013, "Nonlinear Transient Dynamics of Pendulum Torsional Vibration Absorbers—Part I: Theory," ASME J. Vib. Acoust., **135**(1), p. 011017.
[9] Monroe, R. J., and Shaw, S. W., 2013, "Nonlinear Transient Dynamics of Pendulum Torsional Vibration Absorbers—Part II: Experimental Results," ASME J. Vib. Acoust., **135**(1), p. 011018.
[10] Ishida, Y., 2012, "Recent Development of the Passive Vibration Control Method," Mech. Syst. Signal Process., **29**(1), pp. 2–18.
[11] Heymans, N., 2004, "Fractional Calculus Description of Non-Linear Viscoelastic Behavior of Polymers," Nonlinear Dyn., **38**(1–4), pp. 221–231.
[12] Pritz, T., 1996, "Analysis of Four-Parameter Fractional Derivative Model of Real Solid Materials," J. Sound Vib., **195**(1), pp. 103–115.
[13] Pritz, T., 2003, "Five-Parameters Fractional Derivative Model for Polymeric Damping Materials," J. Sound Vib., **265**(5), pp. 935–952.
[14] Wu, J., and Shangguan, W. B., 2008, "Modeling and Applications of Dynamic Characteristics for Rubber Isolators Using Viscoelastic Fractional Derivative Model," Eng. Mech., **25**(1), pp. 161–166 (in Chinese).
[15] Bahraini, S. M. S., and Eghtesad, M., 2013, "Large Deflection of Viscoelastic Beams Using Fractional Derivative Model," J. Mech. Sci. Technol., **27**(4), pp. 1063–1070.
[16] Berg, M., 1998, "A Non-Linear Rubber Spring Model for Rail Vehicle Dynamics Analysis," Veh. Syst. Dyn., **30**(4), pp. 197–212.
[17] Sjoberg, M., and Kari, L., 2002, "Non-Linear Behavior of a Rubber Isolator System Using Fractional Derivatives," Veh. Syst. Dyn., **37**(3), pp. 217–236.
[18] Sjoberg, M., and Kari, L., 2003, "Nonlinear Isolator Dynamics at Finite Deformations: An Effective Hyperelastic, Fractional Derivate, Generalized Friction Model," Nonlinear Dyn., **33**(3), pp. 323–336.
[19] Wu, J., and Shangguan, W. B., 2010, "Dynamic Optimization for Vibration Systems Including Hydraulic Engine Mounts," J. Vib. Control, **16**(11), pp. 1577–1590.
[20] Shangguan, W. B., and Wu, J., 2008, "Modeling of Dynamic Performances for Hydraulic Engine Mounts Using Fractional Derivative and Optimisation of Powertrain Mounting Systems," Int. J. Veh. Des., **47**(1–4), pp. 215–233.
[21] Honda, Y., and Saito, T., 1987, "Dynamic Characteristics of Torsional Rubber Dampers and Their Optimum Tuning," SAE Technical Paper No. 870580.
[22] Shangguan, W. B., and Lu, Z. H., 2004, "Experimental Study and Simulation of a Hydraulic Engine Mount With Fully Coupled Fluid Structure Interaction Finite Element Analysis Model," Comput. Struct., **82**(22), pp. 1751–1771.
[23] Amin, A. F. M. S., Lion, A., Sekita, S., and Okui, Y., 2006, "Nonlinear Dependence of Viscosity in Modeling the Rate-Dependent Response of Natural and High Damping Rubbers in Compression and Shear: Experimental Identification and Numerical Verification," Int. J. Plast., **22**(9), pp. 1610–1657.
[24] Yeoh, O. H., 1990, "Characterization of Elastic Properties of Carbon-Black-Filled Rubber Vulcanizates," Rubber Chem. Technol., **63**(5), pp. 792–805.
[25] Garcia, T. M. J., Kari, L., Vinolas, J., and Gil-Negrete, N., 2007, "Torsion Stiffness of a Rubber Bushing: A Simple Engineering Design Formula Including the Amplitude Dependence," J. Strain Anal. Eng. Des., **42**(1), pp. 13–21.
[26] Wang, L., Wang, J., and Hagiwara, I., 2005, "An Integrated Characteristic Simulation Method for Hydraulically Damped Rubber Mount of Vehicle Engine," J. Sound Vib., **286**(4), pp. 673–696.